

Preparation and Characterization of a Novel Chemically Crosslinked Chitosane-g-Polyacrylamide Hydrogel as a Promising Adsorbent for the Removal of Methylene Blue from Aqueous Solutions

H. Sehil^{a,*}, M. Badaoui^b, and A. Chougui^b

^aDepartment of Chemistry, Faculty of Sciences of the Matter, University of Tiaret, BP P 78, Zaaroura, Tiaret, Algeria

^bSynthesis and Catalysis Laboratory, University of Tiaret, BP P 78 Zaaroura, Tiaret, Algeria

*e-mail: hafida.sehil@univ-tiaret.dz

Received June 1, 2021; revised July 22, 2021; accepted September 5, 2021

Abstract—The present study aims primarily to develop a new three-dimensional chitosan-graft-polyacrylamide hydrogel through radical polymerization using sodium trimetaphosphate as a crosslinking agent. The structural confirmation of the synthesized hydrogel was carried out by Fourier transform infrared spectroscopy and X-Ray diffraction analysis. In addition, the thermal behavior of the above hydrogel was investigated using thermogravimetric analysis and differential thermal analysis. Moreover, the kinetics and swelling behavior of the resulting product were also enquired. The hydrogel obtained was used as an adsorbent to remove cationic dyes from aqueous solutions. It was found that the hydrogel possessed a high adsorption capacity that reached 872 mg/g under optimum conditions. Thus, kinetic, thermodynamic, and adsorption isotherm models were employed to describe the adsorption process of methylene blue onto the chitosan-based hydrogel. The results obtained suggested that the adsorption of methylene blue onto the hydrogel is fitted well with the pseudo-second-order and Freundlich models. According to the thermodynamic studies, it was revealed that the adsorption of methylene blue onto hydrogel was a spontaneous and exothermic process.

DOI: 10.1134/S1560090421060269

INTRODUCTION

It is widely admitted that the recent technological advances as well as the rapidly increasing world population have skyrocketed industrial pollution. Indeed, over the last few years, the manufacturing of large numbers of diverse industrial goods has generated huge quantities of waste that could threaten the public health as well as the environment. For example, the textile industry was found to be one of the most polluting sources, in terms of volume and composition of wastewater discharged. Indeed, textile manufacturing companies alone can globally consume more than 7×10^5 tons of dye; however, 10 to 50% of that quantity is disposed of as effluents during the dyeing process [1]. It is well acknowledged that the textile industry is one of the major consumers of water; it discharges various organic dyes in the environment. In addition, textile dyes are viewed as dangerous substances for the public health and the environment as well [2, 3].

It is well known that these dyes include aromatic complex structures as well as azo groups. It should be noted that, under normal conditions, most of these azo groups are hardly biodegradable substances; they are stable and can have severe effects on human health [4]. In particular, it was shown that methylene blue (MB) is one of the most commonly used and environ-

mentally hazardous dyes [5, 6]. In this context, the results of some studies showed that this dye may cause breathing problems, retching, cyanosis, vomiting, permanent eye burns, jaundice, and mental confusion for humans as well as for animals [7, 8]. Moreover, MB can inhibit the diffusion of sunlight in water, which can seriously threaten the aquatic life [9]. It is therefore highly recommended to develop appropriate treatment methods for the removal of dyes from contaminated wastewater before discharge.

Lately, different treatment methods including oxidation, coagulation, photocatalysis, membrane separation, biological treatment, and adsorption, have been applied for the removal of dyes from wastewaters [10–13].

Adsorption is considered as the most promising approach for efficient removal of toxic dyes from wastewater. The adsorption technique turned out to be very attractive due to its high efficiency, convenience, easy operation, simplicity of design, and low cost [14–17]. However, it is worth stressing that the performance and effectiveness of this adsorption technique depends, in a preponderant manner, on the nature of the support used as adsorbent, and particularly on its cost, availability, and regeneration [18]. Based on the above, researchers have been increasingly interested in

developing new efficient, stable and recyclable adsorbents based on biomaterials (chitosan, alginate, starch, etc.) and their derivatives [19–22].

Over the last few years, special attention has been paid to biopolymer-based hydrogels and their applications in various fields, such as medicine, cosmetics, personal care products, industrial wastewater treatment, agriculture and environmental remediation [23–25].

As far as wastewater treatment is concerned, it was revealed that hydrogels, used for the adsorption of synthetic dyes from aqueous solutions, exhibited a quite high performance because they possess a high adsorption efficiency [26, 27] and great recovery capacity; they can be regenerated and reused after several cycles [28]. It should be added that chemically cross-linked polysaccharides have numerous advantages, such as rapid adsorption kinetics, easy operation and important diffusion properties due to the hydrophilic character of the polysaccharide repeating units. These materials show a very high swelling capacity in water [29], and therefore their networks are sufficiently developed to allow rapid diffusion of pollutants [30]. On the other hand, the grafting of amines [31] or carboxyl [32] functional groups on polysaccharides turned out to be a very effective method for these purposes. Furthermore, after adsorption, the cross-linked polymers can easily be regenerated [33]. One of these polysaccharides, i.e. Chitosan (Cs) which is the most abundant biopolymer after cellulose, have been widely investigated and used, along with its derivatives, for the treatment of dyeing wastewater because Chitosan chains have a great amount of amines and hydroxyl groups [34].

The present paper aims at developing a newly fabricated chitosan-based hydrogel that was prepared by grafting polyacrylamide on chitosan chains using ammonium persulfate (APS) and sodium trimetaphosphate (STMP) as initiator and cross-linker, respectively, in an aqueous medium.

The synthesized hydrogel was characterized by Fourier transform infrared (FTIR) spectroscopy, X-Ray diffraction (XRD), thermal gravimetric analysis (TGA), differential thermal analysis (DTA); the swelling properties of the hydrogel were also assessed. Furthermore, the MB removal capacity of this hydrogel from aqueous solutions was evaluated. Moreover, the adsorption kinetics, isotherms, thermodynamics and various factors affecting the sorption process were also investigated.

EXPERIMENTAL

Materials

Chitosan (poly(D-glucosamine)) was supplied by Sigma-Aldrich Corporation. Acrylamide (ACM) was purchased from Fluka and sodium chloride from BIO-

CHEM Chemopharma. Ammonium persulfate (APS) and hydrochloric acid were obtained from Merck and acetic acid was from Prolabo. Methylene blue (MB), sodium hydroxyde, sodium trimetaphosphate (STMP) were provided by Sigma-Aldrich. Double-distilled water was used for the preparation of the synthetic wastewater solutions.

Synthesis of Hydrogel (Cs-STMP-ACM)

The hydrogel (Cs-STMP-ACM) was prepared using sodium trimetaphosphate (STMP) as a cross-linker and ammonium persulfate (APS) as an initiator in an aqueous medium. In addition, the grafting of the acrylamide monomer onto crosslinked chitosan was performed using the free-radical copolymerization technique according to the following procedure. Chitosan (2 g) was introduced into a three-neck reactor equipped with a mechanical stirrer, along with 60 mL of a 5% (v/v) acetic acid solution. After complete dissolution of chitosan, the STMP solution (0.1 M, pH = 12) was added to the mixture. After stirring for 30 min, the reactor was immersed into a thermostatted water bath that was preset to the temperature of 65°C. Next, the APS solution (0.1 g) and ACM (1 M) were added to the reaction mixture. Afterwards, the resulting hydrogel was immersed into an excess of non-solvent (200 mL of ethanol) for 3 h, for dehydration. Then, the hydrogel was filtered and immersed once more into 100 mL of ethanol, for 24 h. Finally, after filtration, the hydrogel was dried at 45°C, during 48 h. It was then ground and the powder obtained was stored.

Regeneration of Adsorbent

The regeneration of the adsorbent after the adsorption experiments was accomplished by immersing the hydrogel laden with MB into a 0.1 M HCl solution, under continuous shaking, at room temperature, for 24 h. The HCl solution was used as the desorption agent. Afterwards, the hydrogel was separated by filtration and washed with distilled water while still on the magnetic shaker, until reaching a neutral pH. The adsorbent was regenerated after three cycles [35].

Methods and Characterization

The Fourier transform infrared spectrophotometer (Bruker Alpha-P) was used to examine the functional groups over the frequency range from 400 to 4000 cm^{-1} . X-Ray diffraction (XRD) analyses were performed by means of a Rigaku MiniFlex 600 XRD Benchtop X-ray diffractometer. Thermogravimetric analysis (TGA) and differential thermal analysis (DTA) were realized using a LABSYS evo TGA STA DTA/DSC—Setaram Instrument. UV–Vis-2401PC-SHIMADZU spectrophotometer was used to determine the methylene blue concentration in the supernatant solution before and after adsorption, at 664 nm.

Point of zero charge (pH_{pzc}) is a very important parameter in adsorption phenomena. It indicates the pH at which the adsorbent surface is electrically neutral. The pH_{pzc} of the prepared hydrogel was determined as follows. First, a series of 50 mL of 0.01 mol/L NaCl solutions were placed into closed conical flasks; next the pH of these solutions was adjusted to remain within the range 2–10. Then, 0.05 g of the adsorbent was introduced into each flask which was put under agitation, at room temperature. The final pH was then measured after 48 h, and the pH_{pzc} was then determined as the point where the curve representing the variation of $\text{pH}_{\text{initial}}$ against pH_{final} crosses the line for which $\text{pH}_{\text{initial}} = \text{pH}_{\text{final}}$ [36].

The amount of 0.05 g of the prepared hydrogel was immersed, at room temperature, into deionized water (250 mL) until the swelling equilibrium was reached. The swelling ratio Q was obtained gravimetrically; it was calculated using the following equation:

$$\% Q = \frac{m_s - m_d}{m_d} \times 100, \quad (1)$$

where m_s and m_d are the weights of swollen hydrogel and dry hydrogel, respectively.

For the purpose of studying the effect of pH on the swelling behavior, a mass of 0.05 g of dried hydrogel was immersed into various solutions with pH values ranging from 1.5 to 10, for 48 h, at the temperature of 25°C. It should be noted that NaOH and HCl were utilized in order to adjust the pH of the buffer solution.

The adsorption kinetics is the measure of the adsorption uptake with respect to time. It was assessed using a series of batch adsorption experiments, which were carried out into a set of 250 mL conical flasks with glass stoppers, at specific temperature and pH. Each one of these flasks contained 100 mL of various solutions with different MB concentrations, along with a known amount of hydrogel. These flasks were then placed on a magnetic shaker (500 rpm). In addition, when equilibrium was reached, the adsorbent was separated from the aqueous solutions using a membrane filter with 0.22 μm pore size. Further, the residual MB solution was examined by means of a UV–Vis spectrophotometer.

It is worth indicating that the sorption experiments were conducted for the purpose of optimizing different parameters like the contact time, dye concentration, adsorbent amount, initial pH of solution, and temperature. It should be noted that the effect of contact time on adsorption was determined at pH 6 and 25°C, by immersing 0.1 g of adsorbent in a solution containing methylene blue (MB) with concentration 100 mg/L (100 mg/L MB solution); this effect was determined at different times between 1 and 80 min. Then, the effects of the initial MB concentrations, i.e. 100, 200, 300 and 400 mg/L, were investigated under the same conditions of contact time. On the other hand, in order to enquire the effect of the sorbent

mass, different sorbent masses, between 0.04 and 0.1 g, were mixed with 400 mg/L MB solutions at pH = 6, and at temperature 25°C. The effect of initial pH was also enquired by adding 0.4 g of adsorbent to 400 mg/L MB solutions, at different pH values from 1 to 10.

In the end, experiments were carried out by adding 0.04 g of adsorbent to MB solutions at 400 mg/L with a pH = 10 and at different temperatures (25, 40, 50 and 60°C).

Furthermore, the adsorption capacity of the adsorbent and the percentage removal of MB were calculated at equilibrium, using Eqs. (1) and (2), respectively.

$$q = \frac{(C_0 - C_e)V}{m}, \quad (2)$$

$$\%MB = \frac{C_0 - C_e}{C_0} \times 100, \quad (3)$$

where m (g) is the mass of the adsorbent, V (L) is the volume of solution, C_0 (mg/L) is the initial concentration of MB, C_e (mg/L) is equilibrium concentration of MB.

With regard to the isotherm studies, the adsorption experiments were accomplished at a fixed temperature, by mixing 0.04 g of hydrogel with different MB concentrations (100–400 mg/L) in a thermostatted shaking bath. Once equilibrium was reached, the suspension was filtered and the MB concentrations were determined.

RESULTS AND DISCUSSION

Characterizations

The FTIR spectra of the prepared hydrogel (Cs-STMP-ACM) and pure chitosan (Cs) are shown in Fig. 1.

The FTIR spectrum of chitosan shows some characteristic absorption bands. The range 3450–3200 cm^{-1} corresponds to the stretching vibrations of O–H and N–H. The extension vibration of N–H at 1632 cm^{-1} due to N–H bending vibrations indicates the presence of NH_2 , while that observed at 1024 cm^{-1} corresponds to the vibrations of –C–O–C bond [23]. IR spectrum of modified chitosan presents new bands. The first one, which is assigned to P=O, is located between 1100 and 1200 cm^{-1} , while the second, which is attributed to P–O, is between 900–1050 cm^{-1} . These two bands confirm the crosslinking of chitosan by STMP [37]. The spectrum shows a relatively strong band at 3361 cm^{-1} that can be assigned to the symmetric stretching vibrations of the – NH_2 group on the polyacrylamide chains. The band at 3256 cm^{-1} corresponds to the stretching of – NH_2 in the ACM molecules corresponding to the hydrogen bonding state. In addition, the characteristic band of the carbonyl group

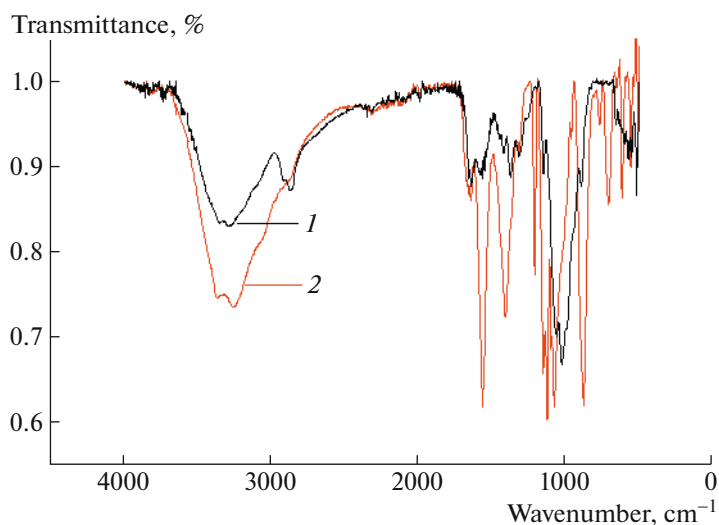


Fig. 1. FTIR graph of (1) Cs and (2) Cs-STMP-ACM.

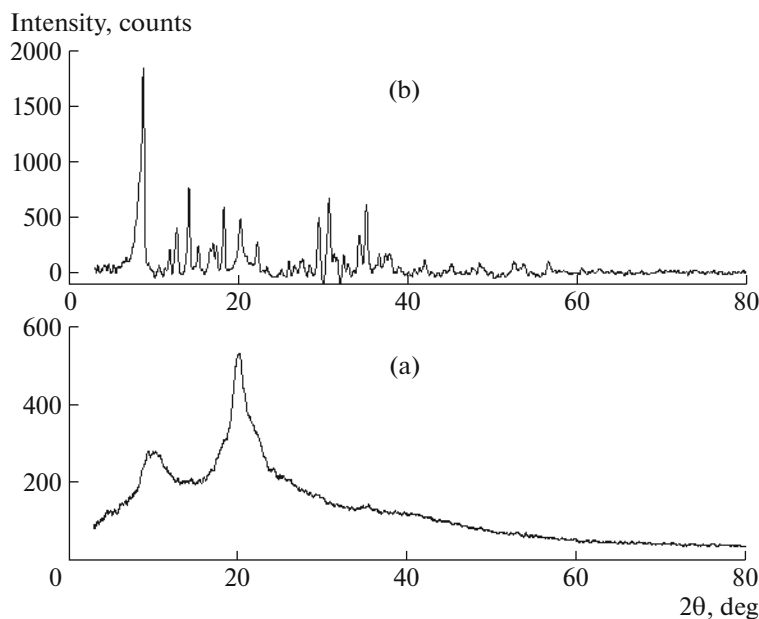


Fig. 2. XRD pattern of (a) Cs and (b) Cs-STMP-ACM.

(C=O) is observed at 1656 cm^{-1} . These three bands confirm the grafting of polyacrylamide on the chitosan chains [38].

Figure 2 shows the X-ray diffraction patterns of chitosan samples. The diffractogram of pure chitosan exhibits two wide peaks at $2\theta = 9.2^\circ$ and 20° that coincide with forms I and II of the crystal structure [39, 40]. Note also that the large peak observed in chitosan at $2\theta = 20^\circ$ becomes weaker and the one at $2\theta = 9.2^\circ$ becomes more intense in the modified chitosan (Cs-STMP-ACM). These findings suggest that the crystalline structure of the new material has changed. This is

certainly due to the incorporation of phosphorus bridges between the chitosan chains.

Figure 3 illustrates the TGA curves of different samples respectively. These curves were registered at different heating rates, in the temperature interval from 25 to 800°C . It is worth noting that the TGA curves of the investigated samples showed two significant weight loss steps, which were recorded first within the temperature interval between 105 and 120°C . These losses, which could be estimated at about 10 to 15%, are due to desorption of water that was physisorbed on the surface of different samples. Additional losses occur at 300 and 252°C for both Cs

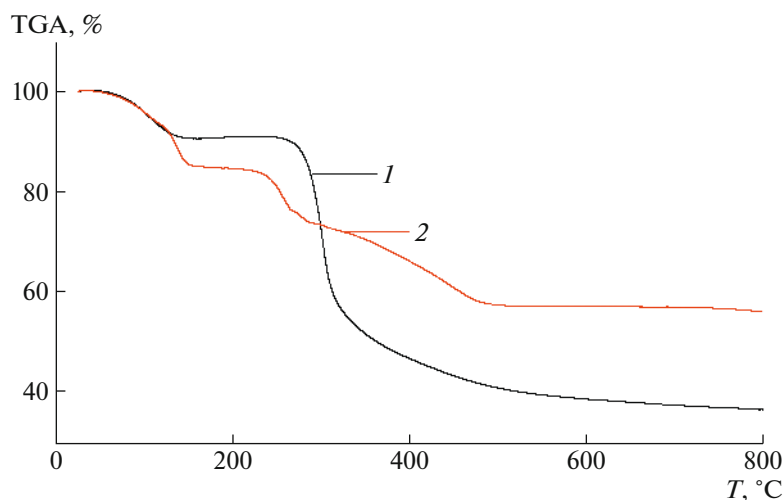


Fig. 3. TGA thermogram of (1) Cs and (2) Cs-STMP-ACM.

and Cs-STMP-ACM. These losses can be assigned to the decomposition of the polymer chains through the degradation of the glycosidic bond (C–O–C) of the material under investigation. These results are in good agreement with those previously reported by Corazzari et al. [41].

Close examination of the DTA thermogram of the studied samples (Cs and Cs-STMP-ACM) depicted in Fig. 4 reveals the presence of two thermal events. The first one refers to the endothermic peak, with T_{onset} between 104 and 137°C, and the second one to the exothermic peak and was recorded within the interval from 320 to 260°C, for Cs and Cs-STMP-ACM, respectively. This is consistent with the findings of other studies reported in the literature [42]. In addition, the area under the endothermic peak (ΔH) depends on the water holding capacity of Cs and Cs-STMP-ACM as well as on the strength of chitosan-water interaction, while the area under the peak of the second thermal event corresponds to the overall exothermic effect that is attributed to the decomposition of hydrogel (Cs-STMP-ACM). It should be mentioned that the position of the second peak shifts to lower temperatures in Cs-STMP-ACM, indicating that the thermal stability of chitosan dropped after modification.

It is worth noting that the most important parameter that controls the adsorption process is the pH of the aqueous solution as the surface charge of the adsorbent is affected by the change in the pH of the solution through protonation and deprotonation phenomena [43]. In order to elucidate the role of the net surface charge of the adsorbent in the fixation of the dye, it was decided to determine the point of zero charge (pH_{pzc}) of the hydrogel.

Figure 5 indicates that the pH_{pzc} of (Cs-STMP-ACM) was equal to 2.95. For pH values higher than

the pH_{pzc} , the hydrogel acquires negative surface charges due to the adsorption of OH^- ions or to the deprotonation of phosphoric acid, which promotes the adsorption of the cationic adsorbate (MB) on account of the electrostatic attraction. However, for $\text{pH} < \text{pH}_{\text{pzc}}$, the surface of the adsorbent is positively charged due to the adsorption of hydrogen ions H^+ from the solution and also to the protonation of the amine functions.

Swelling Behavior of Hydrogel Cs-STMP-ACM

The results of the swelling study indicated that the hydrogel exhibited a 620% swelling percentage, after 100 min. Beyond this period, a constant swelling level was observed when the equilibrium swelling was reached, as indicated in Fig. 6.

It was observed that the swelling rate increased as the pH value passed from 6 to 10 (Fig. 7). The increase in pH values favored the ionization of acid groups in the hydrogel structure and consequently enhanced the electrostatic repulsions between charged sites POO^- . Moreover, this facilitated the penetration of water into the hydrogel and therefore increased its swelling rate [37]. It is important to mention that a second swelling rate growth occurred when the pH value dropped from 6 to 1.5. This swelling increase could be justified by the protonation of NH_2 groups, which caused the swelling to rise due to electrostatic repulsions.

In order to study the swelling mechanism of the hydrogel, swelling kinetics was investigated. According to Pourjavadi and Mahdavinia, for the first-order kinetic model, and before reaching equilibrium, the swelling rate was directly dependent on the amount of water that the hydrogel is supposed to absorb [44]. The first-order swelling kinetics may be expressed as follows:

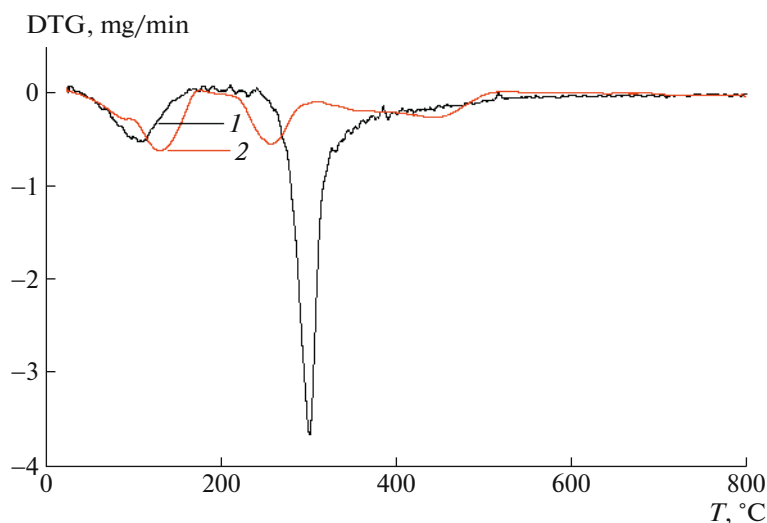


Fig. 4. DTA thermogram of (1) Cs and (2) Cs-STMP-ACM.

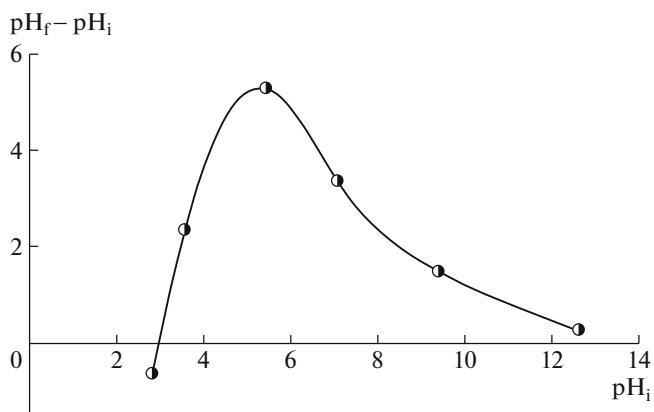


Fig. 5. Determination of pHpzc of Cs-STMP-ACM hydrogel.

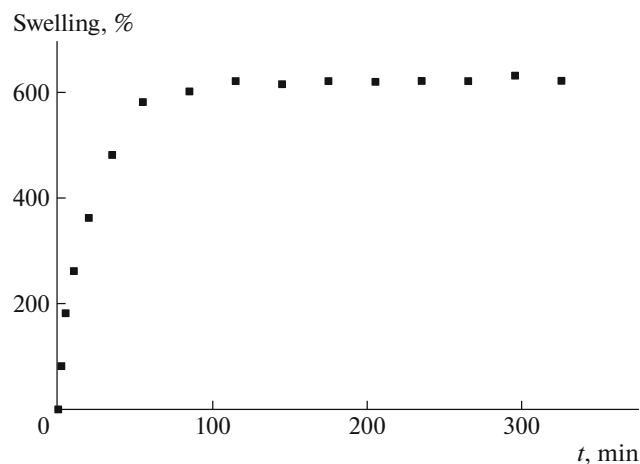


Fig. 6. Profile of swelling of Cs-STMP-ACM hydrogel in deionized water versus time.

$$\ln \frac{m_e}{m_e - m_t} = kt, \quad (4)$$

where m_t and m_e are the hydrogel weights at time t and at equilibrium time, respectively, and k is the reaction rate constant. The fit of this first-order kinetic model was evaluated and, as is illustrated in Fig. 8a, the plot of $\ln(m_e/(m_e - m_t))$ versus t is not a straight line. It can therefore be stated that the swelling process did not follow the first-order absorption kinetic model, which was certainly due to the different chemical groups attached to the hydrogel, as these chemical compounds engender various polymer-solvent interactions.

With regard to the second-order adsorption kinetic model, it was evaluated according to the following equation:

$$\frac{t}{m_t} = \frac{1}{km_e^2} + \frac{1}{m_e}t. \quad (5)$$

According to Fig. 8b, the swelling data allowed obtaining straight lines for the plot of t/m_t as a function of time. Though the experimental value of the hydrogel mass at equilibrium m_e was found equal to 6.3 g/g, the theoretical value was estimated at 6.5 g/g, with a correlation coefficient of 0.9991. It can therefore be concluded that the second-order kinetic model describes quite well the swelling of the hydrogel under study [45].

Parameters Affecting the Methylene Blue Adsorption

Figure 9 shows that after 5 min of contact time, the adsorption of MB reached 85% of the equilibrium adsorption capacity q_e . This may be attributed to the

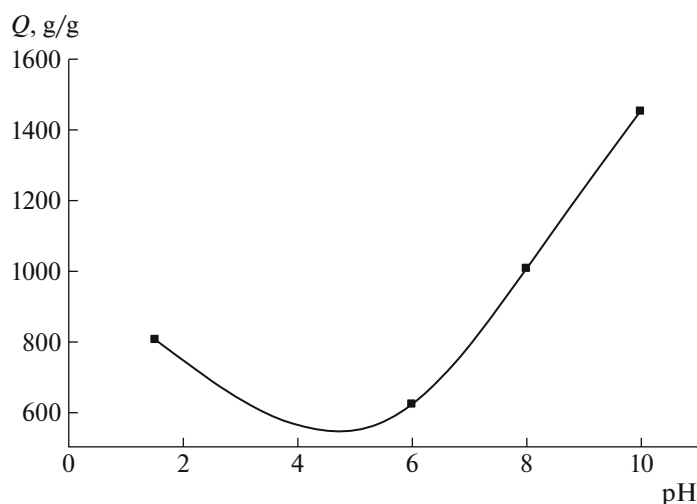


Fig. 7. Effect of pH on hydrogel swelling.

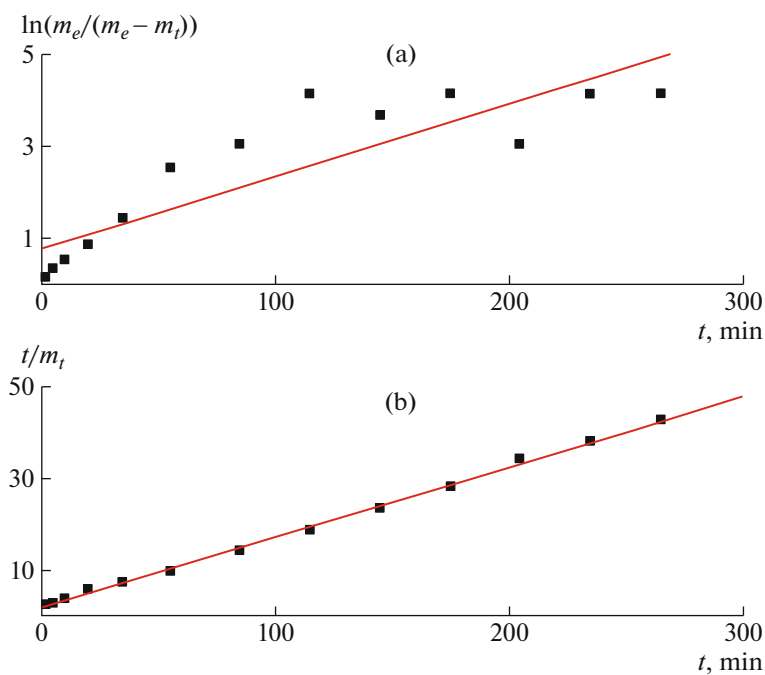


Fig. 8. Swelling kinetics were examined by (a) pseudo-first order ($y = 0.7716 + 0.0157x$, $R^2 = 0.8824$) and (b) pseudo-second-order models ($y = 1.8379 + 0.1530x$, $R^2 = 0.9991$).

rapid dilution of methylene blue and to its adsorption on the adsorbent surface, and also to the interactions between MB and the adsorbent surface. For a faster rate, the adsorption sites became fully saturated and equilibrium was reached after 10 min. Usually, the adsorption mechanism, which is directly linked to the adsorption of dyes on porous solids, follows different steps [46]. First, the dye molecules move from the solution onto the surface of the adsorbent. Then these molecules diffuse in the region between the solution and solid to eventually interact with the adsorption

sites that are located on the adsorbent surface. Finally, these dye particles penetrate into the pores of the solid. In order to analyze the adsorption kinetics of MB onto hydrogel Cs-STMP-ACM, it was deemed important to apply the pseudo-first order [47] and pseudo-second order [48] kinetic models. Eqs. (6) and (7) express the linear first-order and second-order kinetic forms, respectively.

$$\ln(q_e - q_t) = \ln q_e - k_1 t, \tag{6}$$

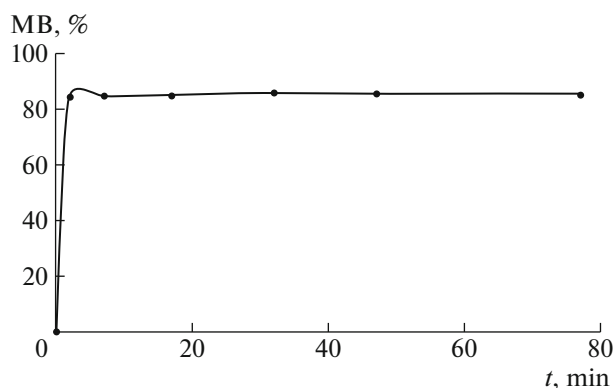


Fig. 9. Effect of contact time.

$$\frac{t}{q_t} = \frac{1}{k_2 q_e^2} + \frac{t}{q_e} \quad (7)$$

Note that q_e and q_t (mg/g) are the sorption capacities at equilibrium and at time t , respectively, while k_1 and k_2 are respectively the rate constants of the first-order and second-order models.

The fit of these models was assessed based on the linear plots depicted in Fig. 10 and the kinetic parameters are summarized in Table 1. According to Fig. 10, and based on the kinetic parameters presented in Table 1, it may be said that the experimental data for the adsorption of MB on hydrogel fits well with the pseudo-second order kinetic model [49]. It is worth mentioning that the pseudo-second order kinetic model considers that chemisorption could be the rate-limiting step that satisfies the adsorption process [48]. In this case, it is assumed that valence forces are involved in chemical bonding due to the electrons exchanged between the hydrogel and methylene blue (MB). In addition, it can be said that the adsorption rate depends on the sorption capacity of the adsorbent but not on the adsorbate concentration [50].

The influence of the initial MB concentration on the adsorption performance of the hydrogel is presented in Fig. 11. It was observed that, when the initial concentration increases from 100 to 400 mg/L, the adsorption capacity of the hydrogel for the MB dye augmented from 85 to 344 mg/g. This means that the adsorption capacity increase took place for high MB

concentrations, which was probably due to the fact that at low MB concentrations, the adsorption sites on the adsorbent were not entirely occupied [51].

Figure 12 shows the influence of the hydrogel mass on the removal of MB from an aqueous solution. In fact, this figure reveals that the increase in the hydrogel mass leads to a reduction in the adsorption capacity, i.e. better dye removal. Indeed, a promising adsorbent material has the ability to eliminate important amounts of dye at low doses. The sorption capacity decreased from 852 to 344 mg/g as the mass of the sorbent went from 0.04 to 0.1 g. As the adsorbent mass went up, surface interactions between the adsorbent particles led to aggregations. This caused the number of adsorption sites to diminish and consequently the adsorption efficiency decreased [52]. Furthermore, the diminution in adsorption capacity with increased adsorbent mass could also be assigned to the unsaturated adsorption sites during the adsorption process [53].

The effect of pH on the adsorption capacity was studied under optimal parameter conditions, with the initial MB concentration equal to 400 mg/L and a mass of adsorbent of 0.04 g. The results obtained are presented in Fig. 13. The plotted curve shows that as the pH of the solution increased from 1.5 to 10, the adsorption capacity shifted from 810 to 872. These findings are certainly attributed to the negatively charged adsorbent surface for alkaline pH values; this would promote the electrostatic attraction between the MB cations and the gel surface. On the other hand, under acidic pH conditions, the surface of the gel was positively charged, which engendered electrostatic repulsions between the MB cations and the sorbent surface. Consequently, it can be concluded that there is a better sorption under alkaline pH conditions.

Figure 14 depicts the effect of temperature on the adsorption efficiency of MB onto the hydrogel. It was found that the hydrogel adsorption capacity dropped as the temperature went up. In addition, the adsorption decreased within the temperature range 25–60°C, which means that the adsorption process of MB onto the hydrogel is exothermic.

The lowering in the q_e values at high temperatures can be justified by three principal reasons:

Table 1. Kinetic parameters for different kinetic models

[BM], mg/L	Pseudo-first-order		Pseudo-second-order		q_e^{exp} , mg/g
	K_1 , min ⁻¹	q_e^{cal} , mg/g	K_2 , mg/(g min)	q_e^{cal} , mg/g	
100	0.043	3.9	1.11	86	85
200	0.040	6.5	0.20	172	170
300	0.052	6.5	0.10	260	260
400	0.034	4.5	0.05	345	344

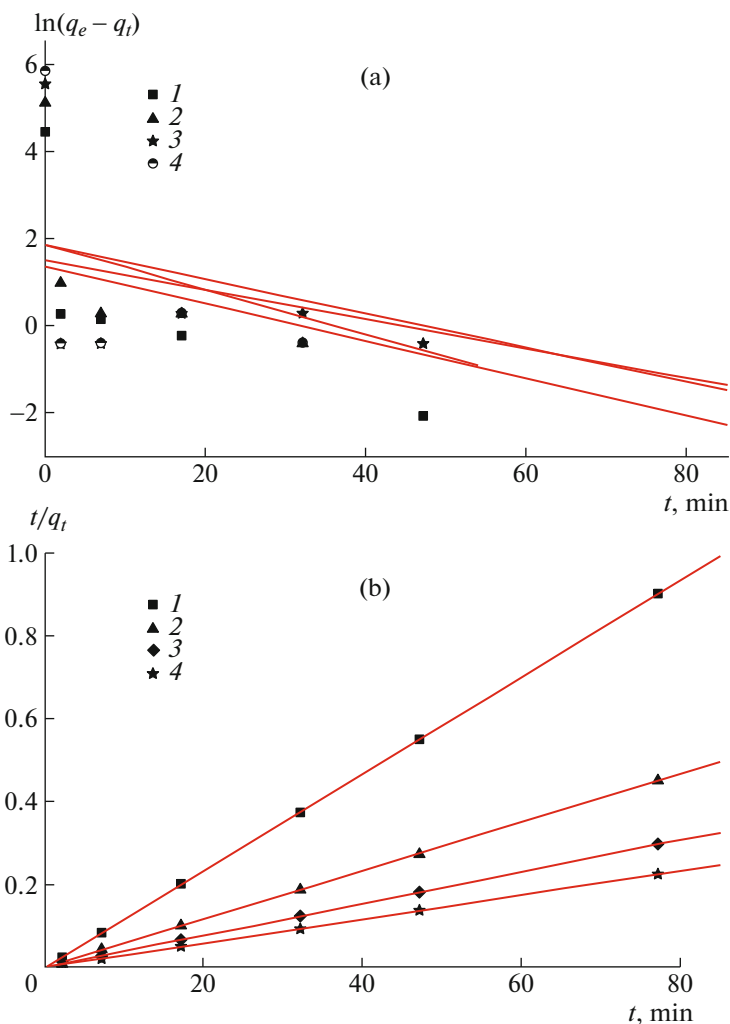


Fig. 10. (a) Pseudo-first and (b) pseudo-second order kinetic model for MB adsorption on the hydrogel prepared: (1) 100, (2) 200, (3) 300, (4) 400 mg/g. (a) (1) $y = 1.3723 - 0.0430x$, $R = -0.6$, (2) $y = 1.8718 - 0.0393x$, $R = -0.5476$, (3) $y = 1.8766 - 0.0519x$, $R = -0.4807$, (4) $y = 1.5155 - 0.0339x$, $R = -0.3944$. (b) (1) $y = 1.2159 \times 10^{-4} + 0.00166x$, $R = 0.9999$, (2) $y = 1.7134 \times 10^{-4} + 0.0058x$, $R = 0.9999$, (3) $y = 1.4842 \times 10^{-4} + 0.00384x$, $R = 0.9999$ (4) $y = 1.5341 \times 10^{-4} + 0.0029x$, $R = 0.9999$.

—High temperatures promote the solubility of MB as well as the solvent-adsorbate interactions that hinder the adsorption process.

—The high kinetic energy of the components involved in the adsorption process weakens the adsorbent–adsorbate interactions.

—The movement of MB particles within the solution decreases their adsorption.

It is interesting to note that several studies have recently reported similar results [54, 55]. It may be concluded that the findings above suggest that the adsorbent designed in this work is highly efficient for the removal of MB from aqueous solutions, under ambient conditions. In general, the adsorption phenomenon is always accompanied by a thermal process that can be either exothermic ($\Delta H < 0$) or endothermic ($\Delta H > 0$) [56]. The measurement of the adsorption

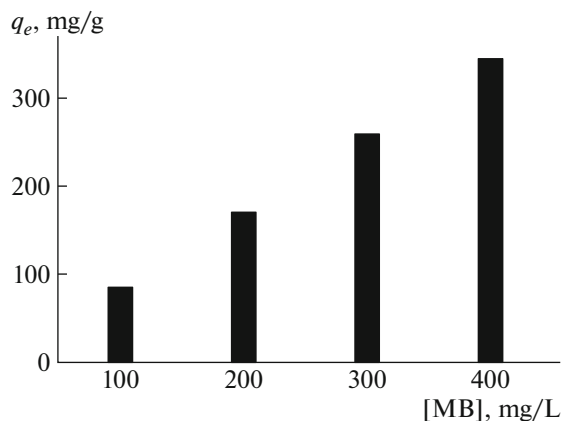


Fig. 11. Effect of initial dye concentration.

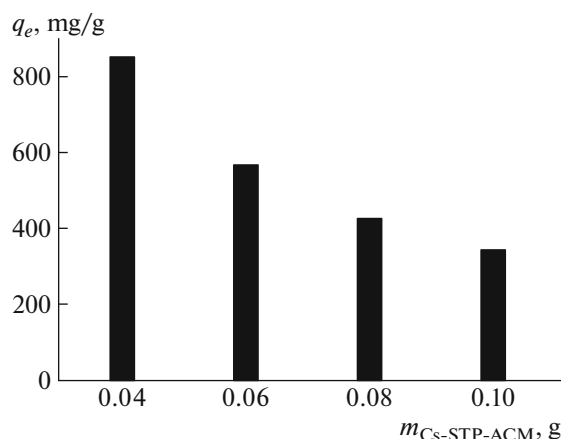


Fig. 12. Effect of adsorbent amount on adsorption capacity of adsorbent.

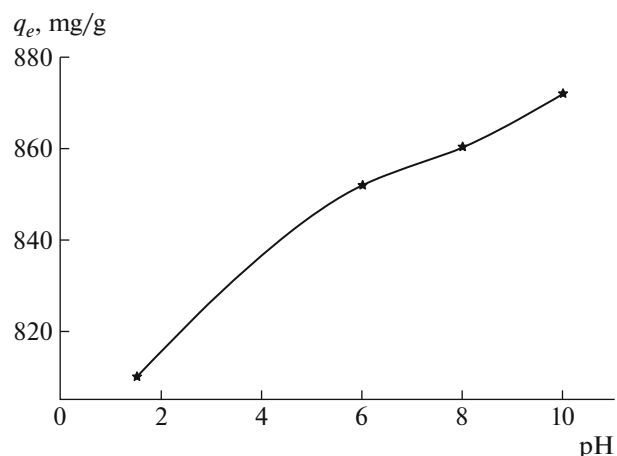


Fig. 13. Effect of pH on adsorption capacity.

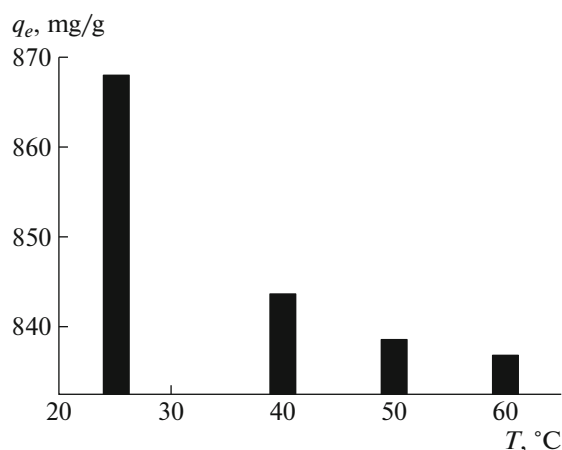


Fig. 14. Effect of temperature on adsorption capacity.

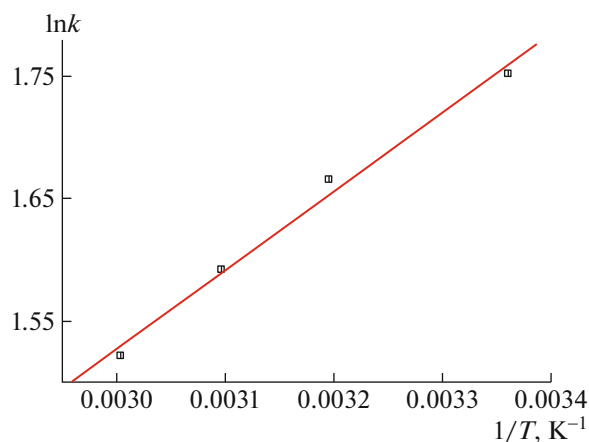


Fig. 15. Plot of $\ln K$ against $1/T$ ($y = -0.4179 + 672.57x$, $R = 0.99$).

heat ΔH is the main criterion that allows making the difference between chemisorption and physisorption. The enthalpy of adsorption ΔH is given by the Gibbs-Helmholtz relation [57] below:

$$\Delta G = -RT \ln K, \quad (8)$$

$$\Delta G = \Delta H - T\Delta S, \quad (9)$$

$$\ln K = \left(\frac{\Delta S}{R}\right) - \left(\frac{\Delta H}{RT}\right), \quad (10)$$

where K is the equilibrium constant $K = C_e/(C_0 - C_e)$, ΔG the free enthalpy (J/mol), ΔH the enthalpy (J/mol), ΔS the entropy (J/(mol K)), T the absolute temperature (K), R the universal gas constant ($R = 8.314 \text{ J/(mol K)}$), and C_0 (mg/L) and C_e (mg/L) the initial and equilibrium concentrations of MB, respectively. Note that the parameters ΔH and ΔS can be determined from the plot of $\ln K$ versus $1/T$ (Fig. 15).

The calculated thermodynamic parameters are listed in Table 2.

From the results obtained, one may say that the negative ΔH values confirm that the dye adsorption on the hydrogel Cs-STMP-ACM is an exothermic process. Low ΔH values ($< 40 \text{ kJ/mol}$) indicate that weak energies are involved in the adsorption of MB, which confirms the physical nature of this process [25, 58]. The negative values of entropy suggest that the adsorption process has favored a reordering of the MB particles on the adsorbent surface. In general, as the fixation of MB molecules to the hydrogel increases the homogeneity of the surface, no significant changes occur in their internal structure [59]. The negative ΔG values given in Table 2 indicate that the process of dye adsorption on the hydrogel is a spontaneous process under different temperature conditions. On the other hand, the process of MB adsorption on the hydrogel appears to be more spontaneous at room temperature,

which is in agreement with the experimental data presented in Fig. 15.

Adsorption Isotherms

The adsorption isotherms are utilized to describe the adsorbate–adsorbent interactions and to find the equilibrium concentration of the adsorbate in solution. Figure 16 presents the amount of adsorbate at equilibrium per unit of adsorbent mass as a function of adsorbate concentration. According to the original classification of adsorption isotherms, established in papers [60, 61], the adsorption isotherm of methylene blue on this hydrogel is of type C.

Many theoretical models have indeed been developed to describe the adsorbate–adsorbent interactions; the most used ones are the Langmuir and Freundlich models. The Langmuir model, which is linked to monolayer surface adsorption comprising a finite number of similar sites, was successfully applied to many real adsorption processes. It is worth indicating that the Freundlich adsorption isotherm model is based on the hypothesis that adsorption takes place on a heterogeneous surface through multilayer adsorption with a non-uniform distribution of sorption heat [62]. The linear forms of Langmuir and Freundlich isotherm models are given by Eqs. (11) and (12), respectively:

$$\frac{C_e}{q_e} = \frac{1}{k_f q_m} + \frac{C_e}{q_m}, \tag{11}$$

$$\ln(q_e) = \ln(k_f) + \frac{1}{n_f} \ln(C_e), \tag{12}$$

where, q_e (mg/g) is adsorption capacity at equilibrium, q_m (mg/g) is maximum adsorption capacity of the hydrogel, C_e (mg/L) is equilibrium concentration of MB, K_L and K_F (L/mg) are Langmuir and Freundlich constants respectively, $1/n$ is the intensity of adsorption.

The use of slopes and intercepts of the linear plottings ($\ln q_e$ against $\ln C_e$) and ($1/q_e$ against $1/C_e$) for the Freundlich and Langmuir models, respectively, allow estimating all the corresponding parameters (Fig. 17). The results are presented in Table 3. The results obtained from the Langmuir model made it possible to observe that the correlation coefficient R is equal to unity. However, the maximum adsorbed quantity q_m of MB could not be calculated, because the intercept of the linear plot of the function $1/q_e = f(1/C_e)$ presented a negative value. This negative value is most likely due to the significance of the isotherm point that corresponds to the high dye concentration. In this case, q_m cannot be determined. Likewise, the parameter K_ℓ which was deduced from q_m could not be determined. Therefore, the Langmuir model cannot be utilized to describe the adsorption isotherms of MB.

Table 2. Thermodynamic parameters of Methylene Blue adsorption on Cs-STMP-ACM

T, K	$\Delta G, kJ/mol$	$\Delta H, kJ/mol$	$\Delta S, J/(mol K)$
298	-4.55		
313	-4.50	-5.59	-3.47
323	-4.46		
333	-4.43		

It can hence be concluded that the experimental data are quite well described by the Freundlich model since the correlation coefficient is equal to unity ($R = 1$). On that account, it can be stated that the Freundlich adsorption isotherm model is the most likely to characterize the adsorption of methylene blue (MB) on the hydrogel. Similarly, this same model better describes this adsorption process as compared to the Langmuir adsorption isotherm model. Furthermore, as the value of $1/n_f$ is equal to unity, it can be confirmed that the adsorption of MB on the hydrogel is a linear process.

Stability Study of the Prepared Hydrogel

In general, a good and promising adsorbent should have the potential to be regenerated and reused in order to meet the low cost requirement; it ought also a high adsorption capacity [63]. Figure 18 shows that after three adsorption-desorption cycles of the dye, the prepared hydrogel still exhibited a high adsorption capacity, which means that this hydrogel can be reused for the removal of dyes. Based on the above findings, it can be concluded that the stable and low cost hydrogel developed in this work can be used as an effective adsorbent for the removal of MB from an aqueous solution.

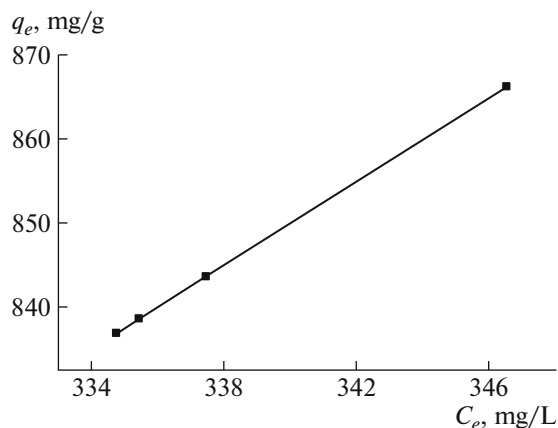
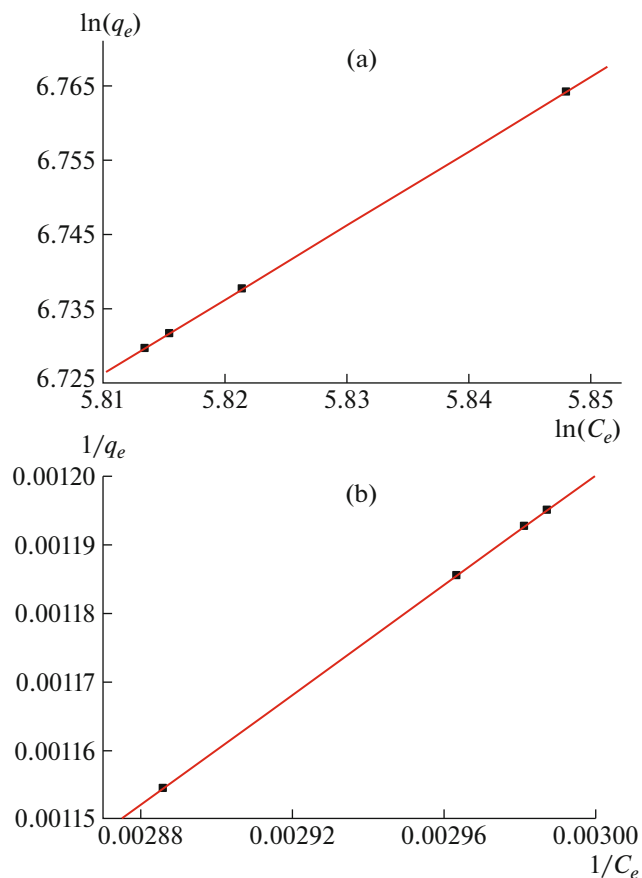
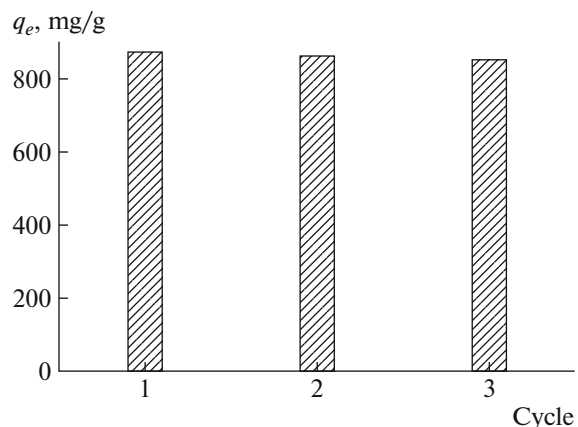


Fig. 16. Adsorption isotherm of MB onto Cs-STMP-ACM.

Table 3. Parameters of Langmuir and Freundlich adsorption isotherms

Freundlich			Langmuir		
k_f	n_f	R	K_ℓ	q_m	R
2.49	1	1	—	—	1

**Fig. 17.** (a) Freundlich plot ($y = 0.91629 + x$, $R = 1$) and (b) Langmuir plot ($y = -1.5418 \times 10^{-8} + 0.410001x$, $R = 1$) of MB adsorption results onto Cs-STMP-ACM.**Fig. 18.** Regeneration study of the adsorbent Cs-STMP-ACM.

CONCLUSIONS

In this study, a new hydrogel was prepared by grafting polyacrylamide on chitosan chains using ammonium persulfate and sodium trimetaphosphate as initiator and cross-linker, respectively, in an aqueous medium. The swelling properties were investigated and it turned out that the swelling ratio of the hydrogel could reach as much as 620% in water. The performance of the hydrogel as an adsorbent to remove MB from an aqueous solution was examined. The hydrogel showed an adsorption capacity greater than 870 mg/g, when 0.04 g of adsorbent was immersed in 100 mL of a MB solution (400 mg/L) at $\text{pH} = 10$ and room temperature. The pseudo-second order model and the Freundlich isotherm model are the most suitable to describe the adsorption process of MB on the hydrogel. The hydrogel can eventually be applied as a potential low-cost adsorbent for wastewater treatment.

CONFLICT OF INTEREST

The authors declare that they have no conflicts of interest.

REFERENCES

1. A. H. Shalla, M. A. Bhat, and Z. Yaseen, *J. Environ. Chem. Eng.* **6**, 5938 (2018).
2. V. K. Gupta and Suhas, *J. Environ. Manage.* **90**, 2313 (2009).
3. P. Wang, M. Cao, C. Wang, Y. Ao, J. Hou, and J. Qian, *Appl. Surf. Sci.* **290**, 116 (2014).
4. Y. He, D. B. Jiang, J. Chen, and Y. X. Zhang, *J. Colloid Interface Sci.* **510**, 207 (2018).
5. S. Chatterjee, A. Kumar, S. Basu, and S. Dutta, *Chem. Eng. J.* **181**, 289 (2012).
6. M. Rafatullah, O. Sulaiman, R. Hashim, and A. Ahmad, *J. Hazard. Mater.* **177**, 70 (2010).
7. B. H. Hameed, A. L. Ahmad, and K. N. A. Latiff, *Dyes Pigm.* **75**, 143 (2007).
8. C. Liu, A. Omer, and X. Ouyang, *Int. J. Biol. Macromol.* **106**, 823 (2018).
9. S. Thakur, S. Pandey, and O. A. Arotiba, *Carbohydr. Polym.* **153**, 34 (2016).
10. J. W. Wang, L. Dai, Y. Q. Liu, R. F. Li, X. T. Yang, G. H. Lan, H. Y. Qiu, and B. Xu, *Carbohydr. Res.* **501**, 108276 (2021).
11. N. Daneshvar, A. R. Khataee, M. H. Rasoulifard, and M. Pourhassan, *J. Hazard. Mater.* **143**, 214 (2007).
12. H. C. Chiu, C. H. Liu, S. C. Chen, and S. Y. Suen, *J. Membr. Sci.* **337**, 282 (2009).

13. Q.S. Liu, T. Zheng, N. Li, P. Wang, and G. Abulikemu, *Appl. Surf. Sci.* **256**, 3309 (2010).
14. M. S. Sajab, C.H. Chia, S. Zakaria, and P. S. Khiew, *Bioresour. Technol.* **128**, 571 (2013).
15. J. W. Fu, Z. H. Chen, M. H. Wang, S. J. Liu, J. H. Zhang, J. N. Zhang, R. P. Han, and Q. Xu, *Chem. Eng. J.* **259**, 53 (2015).
16. Q. Lin, M. Gao, J. Chang, and H. Ma, *Carbohydr. Polym.* **151**, 283 (2016).
17. N. Hou, R. Wang, F. Wang, J. Bai, J. Zhou, L. Zhang, J. Hu, S. Liu, and T. Jiao, *ACS Omega* **5**, 5470 (2020).
18. M. K. Uddin, *Chem. Eng. J.* **308**, 438 (2017).
19. L. Chen, Y. Zhu, Y. Cui, R. Dai, Z. Shan, and H. Chen, *Chem. Eng. J.* **405**, 126953 (2021).
20. H. Geng, Z. Yuan, Q. Fan, X. Dai, Y. Zhao, Z. Wang, and M. Qin, *Carbohydr. Polym.* **102**, 438 (2014).
21. F. A. Ngwabebhoh, M. Gazi, and A. A. Oladipo, *Chem. Eng. Res. Des.* **112**, 274 (2016).
22. Z. Chang, Y. Chen, S. Tang, J. Yang, Y. Chen, S. Chen, P. Li, and Z. Yang, *Carbohydr. Polym.* **229**, 115431 (2020).
23. W. Wang, Y. Zhao, H. Baia, T. Zhanga, V. I. Galvanc, and S. Songb, *Carbohydr. Polym.* **198**, 518 (2018).
24. R. R. Pawar, Lalhmunsiana, P. Gupta, S. Y. Sawant, B. Shahmoradi, and S. M. Lee, *Int. J. Biol. Macromol.* **114**, 1315 (2018).
25. B. C. Melo, F. A. A. Paulino, V. A. Cardoso, A. G. B. Pereira, A. R. Fajardo, and F. H. A. Rodrigues, *Carbohydr. Polym.* **181**, 358 (2018).
26. G. Crini, *Bioresour. Technol.* **97**, 1061 (2006).
27. A. Katzenberg, A. Raman, N. L. Schnabel, A. L. Quispe, A. I. Silverman, and M. A. Modestino, *React. Chem. Eng.* **5**, 377 (2020).
28. Y. Shi, Z. Xue, X. Wang, and A. Q. Wang, *Polym. Bull.* **70**, 1163 (2013).
29. F. M. Soliman, W. Y. H. Guo, M. I. Shinger, A. M. Idris, and E. S. Hassan, *Am. J. Popym. Sci. Technol.* **2**, 11 (2016).
30. X. Qi, R. Liu, M. Chen, Z. Li, T. Qin, Y. Qian, S. Zhao, M. Liu, Q. Zeng, and J. Shen, *Carbohydr. Polym.* **209**, 101 (2019).
31. C. Jeon and W. H. Holl, *Water Res.* **37**, 4770 (2003).
32. A. C. Chao, S. S. Shyu, Y. C. Lin, and F. L. Mi, *Bioresour. Technol.* **91**, 157 (2004).
33. E. Makhado, S. Pandey, P. N. Nomngongo, and J. Ramontja, *J. Colloid Interfaces Sci.* **513**, 700 (2018).
34. Y. Jiang, J. Gong, G. Zeng, X. Ou, Y. Chang, C. Deng, J. Zhang, H. Liu, and S. Huang, *Int. J. Biol. Macromol.* **82**, 702 (2016).
35. H. Dai, Y. Huang, and H. Huang, *Carbohydr. Polym.* **185**, 1 (2018).
36. L. Mounia, L. Belkhirib, J. C. Bollinger, A. Bouzazad, A. Assadid, A. Tirrib, F. Dahmounee, K. Madanie, and H. Reminie, *Appl. Clay Sci.* **153**, 38 (2018).
37. H. Sehil, E. A. Jaudet, Z. Bengharez, and D. L. Cerf, *Biointerface Res. Appl. Chem.* **6**, 1860 (2016).
38. L. H. Gaabour, *Results Phys.* **7**, 2153 (2017).
39. R. A. A. Muzzarelli, P. Morganti, G. Morganti, P. Palombo, M. Palombo, G. Biagini, M. M. Belmonte, F. Giantomassi, F. Orlandi, and C. Muzzarelli, *Carbohydr. Polym.* **70**, 274 (2007).
40. M. T. Yen, J. H. Yang, and J. L. Mau, *Carbohydr. Polym.* **75**, 15 (2009).
41. I. Corazzari, R. Nistico, F. Turci, M. G. Faga, F. Franzoso, S. Tabasso, and G. Magnacca, *Polym. Degrad. Stab.* **112**, 1 (2015).
42. Y. Yuan, B. M. Chesnutt, W. O. Haggard, and J. D. Bumgardner, *Materials* **4**, 1399 (2011).
43. F. C. Wu, R. L. Tseng, and R. S. Juang, *Chem. Eng. J.* **150**, 366 (2009).
44. A. Pourjavadi and G. R. Mahdavinia, *Turk. J. Chem.* **30**, 595 (2006).
45. S. S. Samandari, H. O. Gulcan, S. S. Samandari, and M. Gazi, *Water, Air, Soil Pollut.* **225**, 2177 (2014).
46. A. Dabrowski, *Adv. Colloid Interface Sci.* **93**, 135 (2001).
47. A. E. Rodrigues and C. M. Silva, *Chem. Eng. J.* **306**, 1138 (2016).
48. F. C. Wu, R. L. Tseng, S. C. Huang, and R. S. Juang, *Chem. Eng. J.* **151**, 1 (2009).
49. K. Belloa, B. K. Sarojinia, B. Narayanab, A. Raoc, and K. Byrappad, *Carbohydr. Polym.* **181**, 605 (2018).
50. S. S. Mayakaduwa, P. Kumarathilaka, I. Herath, M. Ahmad, M. Al-Wabel, Y. S. Ok, A. Usman, A. Abduljabbar, and M. Vithanage, *Chemosphere* **144**, 2516 (2016).
51. I. Anil, S. T. Gunday, A. Bozkurt, and O. Alagha, *Nanomaterials* **10**, 131 (2020).
52. W. S. Alencar, E. Acayanka, E. C. Lima, B. Royer, F. E. de Souza, J. Lameira, and C. N. Alves, *Chem. Eng. J.* **209**, 577 (2012).
53. Z. F. Kovacevic, L. Sipos, and F. Briski, *Food Technol. Biotechnol.* **38**, 211 (2000).
54. M. I. El-Khaiary, *J. Hazard. Mater.* **147**, 28 (2007).
55. M. G. Vaz, A. G. B. Pereira, A. R. Fajardo, A. C. N. Azevedo, and F. H. A. Rodrigues, *Water, Air, Soil Pollut.* **228**, 14 (2017).
56. B. Benguella, and A. Yacouta-Nour, *C. R. Chim.* **12**, 762 (2009).
57. K. M. A. ElRahman, A. M. ElKamash, M. R. ElSourougy, and N. M. A. ElMoniem, *J. Radioanal. Nucl. Chem.* **268**, 221 (2006).
58. B. Yan, Z. H. Chen, L. Cai, Z. M. Chen, J. W. Fu, and Q. Xu, *Appl. Surf. Sci.* **356**, 39 (2015).
59. P. Saha, S. Chowdhury, S. Gupta, and I. Kumar, *Chem. Eng. J.* **165**, 874 (2010).
60. C. H. Giles, T. H. MacEwan, S. N. Nakhwa, and D. Smith, *J. Chem. Soc.* **14**, 3973 (1960).
61. N. Nordine, Z. ElBahri, H. Sehil, R. I. Fertout, Z. Rais, and Z. Bengharez, *Appl. Water Sci.* **6**, 349 (2016).
62. S. Kang, Y. Zhao, W. Wang, T. Zhang, T. Chen, H. Yi, F. Rao, and S. Song, *Appl. Surf. Sci.* **448**, 203 (2018).
63. M. Erfani and V. Javanbakht, *Int. J. Biol. Macromol.* **114**, 244 (2018).